

Hierarchical Decoupling Capacitor Optimization for Power Distribution Network of 2.5D ICs with Co-Analysis of Frequency and Time Domains Based on Deep Reinforcement Learning

Yuanyuan Duan, Haiyang Feng, Zhiping Yu, Hanming Wu, Leilai Shao*, Xiaolei Zhu*

Abstract

With the growing need for higher memory bandwidth and computation density, 2.5D design, which involves integrating multiple chiplets onto an interposer, emerges as a promising solution. However, this integration introduces significant challenges due to increasing data rates and a large number of I/Os, necessitating advanced optimization of the power distribution networks (PDNs) both on-chip and on-interposer to mitigate the small signal noise and simultaneous switching noise (SSN). Traditional PDN optimization strategies in 2.5D systems primarily focus on reducing impedance by integrating decoupling capacitors (decaps) to lessen small signal noises. Unfortunately, relying solely on frequency-domain analysis has been proven inadequate for addressing coupled SSN, as indicated by our experimental results. In this work, we introduce a novel two-phase optimization flow using deep reinforcement learning to tackle both the on-chip small signal noise and SSN. Initially, we optimize the impedance in the frequency domain to maintain the small signal noise within acceptable limits while avoiding over-design. Subsequently, in the time domain, we refine the PDN to minimize the voltage violation integral (VVI), a more accurate measure of SSN severity. To the best of our knowledge, this is the first dual-domain optimization strategy that simultaneously addresses both the small signal noise and SSN propagation through strategic decap placement in on-chip and on-interposer PDNs, offering a significant step forward in the design of robust PDNs for 2.5D integrated systems.

Keywords

Power distribution network, Decoupling capacitor, Deep reinforcement learning, Simultaneous switching noise, Impedance, Voltage violation integral

1 Introduction

To address the increasing cost of large Systems-on-Chip (SoCs) on advanced technology nodes, 2.5D integration has emerged as a solution. 2.5D integrated circuits (ICs) enables heterogeneous integration and partitions a monolithic SoC into smaller chiplets, which can be developed independently, reused across multiple products, and implemented using different process technologies [1, 2]. By leveraging the rapid development of 2.5D packaging technology, multiple chiplets can be mounted on a single interposer and connected through microbumps and redistribution layers (RDLs) to build high-performance computing and wafer-scale artificial intelligence (AI) systems.

As data rates continue to increase to hundreds of gigabits per second and the number of input/outputs (I/Os) surges, maintaining the power and signal integrity poses a significant challenge for power distribution network (PDN) design. The 2.5D PDN consists of various components, including on-chip PDNs, an on-interposer PDN, a through-silicon via (TSV) array connecting the interposer and the

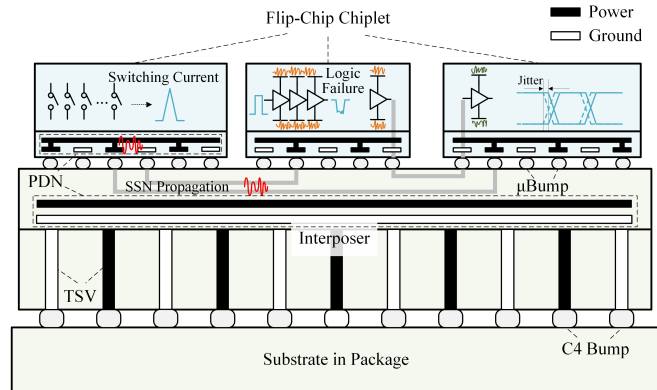


Figure 1: Cross-sectional view of 2.5D system. Large SSN generated can propagate through the hierarchical PDN and cause logic failure and jitter.

package, as well as bumps and decoupling capacitors (decaps) that are widely used to reduce voltage fluctuations and help compensate for transient current demands. The interposer PDN should supply power to the on-chip PDN, which is responsible for delivering voltages to each cell in the design. Therefore, the structure of 2.5D PDN necessitates a hierarchical decap strategy, incorporating both on-chip and on-interposer decaps.

The presence of various components in electronic systems, such as voltage regulator modules (VRMs), decap, and interconnects, introduces inductive and capacitive effects across different frequency ranges [3]. These effects can lead to dynamic voltage fluctuations, commonly known as small signal noise, which has significant implications for system performance and functionality. Moreover, with the escalation in the number of I/Os and the data transmit frequency, simultaneous switching noise (SSN) generates additional voltage fluctuations that may interfere with the operation of other chiplets. The SSN, induced by the large switching currents of multiple I/Os during high-speed data transmission, can propagate through the hierarchical PDN, cause jitter [4] and even logic failure [5, 6], as depicted in Figure 1. Thus, effective strategies to co-optimize the small signal noise and SSN are highly demanded.

PDN analysis is crucial for the design of 2.5D ICs. Frequency-domain impedance often serves as a pivotal criterion for evaluating PDN reliability [7, 8]. Traditional PDN optimization strategies primarily focus on the impedance reduction by implementing additional decaps to alleviate the small signal noise based on the analysis of frequency domain. However, relying solely on meeting target impedance, which guarantees that voltage fluctuation remains within allowable limits, may not sufficiently consider the impact of transient responses on the overall system. The coupled SSN from adjacent chiplets' PDNs, particularly noise propagation through super high bandwidth I/Os, can lead to excessive voltage fluctuation

beyond permissible levels, leading to system failure. Additionally, the high integration and miniaturization of 2.5D systems often result in the routing region occupying a significant portion of the circuit layout, constraining decap placement. Therefore, a comprehensive approach that integrates hierarchical decap placement with considerations of both the small signal noise and SSN is crucial for effectively mitigating power supply noise and ensuring the reliability of PDN designs in 2.5D systems.

In this work, we propose a novel hierarchical decap optimization method for 2.5D systems, integrating both frequency and time domain analyses. It leverages advanced deep reinforcement learning (DRL) techniques and models the load current of the overall system. The main contributions are summarized as follows:

- We present an RL-based approach for the co-optimization of on-chip PDNs and on-interposer PDN decaps to tackle both small signal noise and SSN in 2.5D systems.
- In the frequency domain, this approach optimizes decap placement to reduce the PDN impedance below the target impedance at multiple probing ports (power/ground ports), thus ensuring effective power delivery while avoiding unnecessary over-design.
- In the time domain, we conduct precise simulations of transient currents and introduce the concept of voltage violation integral (VVI). Experiments reveal that despite frequency-domain optimization efforts, voltage violations still occur, indicating instances where voltage fluctuation surpasses acceptable levels. To address this issue, the PDN is refined aiming at minimizing the VVI by strategically implementing additional decaps.
- Extensive validations demonstrate that compared to the frequency-domain optimization alone, the dual-domain optimization strategy can better mitigate the small signal noise and SSN, providing a more robust PDN design for 2.5D ICs.

2 Related Work

In the field of circuits and systems, various methods of decap design optimization have been proposed based on the conventional optimization algorithms, such as the genetic algorithm (GA) [9–11], particle swarm optimization (PSO) algorithm [12, 13] and simulated annealing (SA) algorithm [14–16]. GA-based methods can explore a large search space efficiently, but they may struggle to capture sequential combinatorial relationships between decap assignments and other meta-features, such as the position of probing ports. PSO algorithms, on the other hand, offer fast convergence speeds and simple coding structures. However, they are prone to fall into the local optima, which prevents them from reaching the global optimum solution. Although SA algorithms possess the ability to escape local optima due to their probabilistic acceptance of worse solutions, they have lower convergence rates compared to PSO algorithms and require a good initial solution to perform effectively. None of these optimization algorithms can guarantee finding the optimal solution, especially when dealing with a large number of decap locations. Besides, the optimization time can become problematic, particularly when considering a vast search space. The fusion of differential evolution (DE), which has a strong global search ability, with PSO algorithms enables the optimization of decap designs for 2.5D systems [17]. However, this approach specifically focuses solely on optimizing the on-interposer decap, assuming that chiplets are fully designed and plug-and-play.

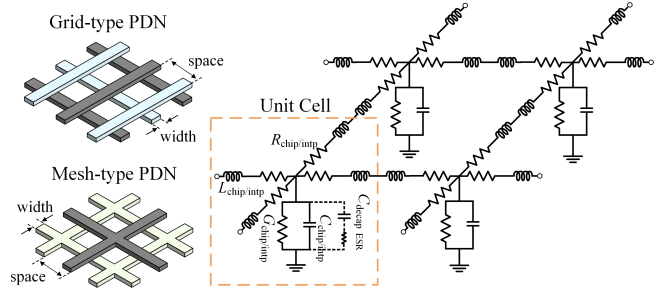


Figure 2: The equivalent model of chiplet and interposer PDNs.

RL has indeed gained traction in addressing complex tasks, especially decap optimization. Several methods utilizing RL for decap optimization have been proposed in the literature [18–21]. Value-based RL methods using the Q-learning algorithm have been explored for decap placement optimization [18, 19]. However, they consider a single probing port and encounter limitations regarding solution space size and high computing costs. To increase the space size and generalization ability, a transformer network-based method for PDN decap optimization of high bandwidth memory (HBM) was proposed [20]. The method can optimize decap design to maximize the reduction of both the self- and transfer impedances seen at multiple ports. Additionally, another RL-based approach [21] optimizes the locations of decaps with different capacitance, considering the complex PDN structure with irregular shapes typical of printed circuit boards (PCBs). This method demonstrates greater scalability compared to the approaches [18–20] that support only one decap capacitance.

Most of the previous decap optimization methods have primarily focused on maximizing the reduction of impedance in the frequency domain [9–21]. However, relying solely on frequency-domain analysis cannot capture the impact of transient responses on the circuit, making it challenging to predict whether the voltage noise meets design requirements. Su *et al.* [22] and Enami *et al.* [23] have investigated the time-domain decap optimization methods for on-chip PDNs only, which are not designated for 2.5D systems.

3 Preliminary Work

3.1 Modeling of 2.5D PDN

Modeling the PDN in a 2.5D IC encompasses various components, such as on-chip PDNs, on-interposer PDN, P/G TSVs, microbumps (μ bumps), and decaps. Each component is modeled individually and subsequently cascaded together.

The on-chip PDN is a grid-type PDN, whereas the interposer PDN is configured with meshed P/G planes. The grid PDN is commonly used in high-speed and high-performance digital systems, consisting of two layers of interwoven P/G planes. In contrast, the meshed PDN comprises two layers, with power planes situated on the upper layer and ground planes on the lower layer. Both the on-chip and on-interposer PDNs can be broken down into a series of unit cells (UCs). Each UC can be represented by unit-length resistance (R), inductance (L), conductance (G), and capacitance (C) in transmission-line (TL) modeling [24, 25], as illustrated in Figure 2. In our experiments, the width and space of on-interposer P/G planes are set to $95 \mu\text{m}$ and $200 \mu\text{m}$, while the width and space of on-chip P/G planes are set to $10 \mu\text{m}$ and $20 \mu\text{m}$.

Table 1: Model parameters of the 2.5D PDN based on 55 nm technology

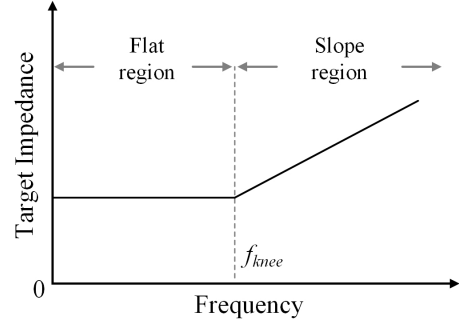
Objective	Parameter	Value
Unit cell of on-chip PDN	R_{chip}	19.11 m Ω
	L_{chip}	8.8 pH
	G_{chip}	$2\pi f C_{chip} \tan(\delta)$
	C_{chip}	17.7 fF
Unit cell of on-interposer PDN	R_{intp}	34.2 m Ω
	L_{intp}	0.63 pH
	G_{intp}	$2\pi f C_{intp} \tan(\delta)$
	C_{intp}	2.79 pF
P/G TSV	R_{TSV}	5.57 m Ω
	L_{TSV}	30 pH
	C_{TSV}	0.24 pF
	R_{bump}	13.85 m Ω
	L_{bump}	2.77 pH
μ bump	$R_{\mu bump}$	0.2 m Ω
	$L_{\mu bump}$	5.69 pH
MOS capacitor	C_{MOS}	14.4 fF/ μm^2
	ESR	24 Ω /pF
MIM capacitor	C_{MIM}	5 fF/ μm^2

* f is the frequency and $\tan(\theta)$ is the loss tangent of dielectric.

TSVs facilitate power transmission between the package and interposer, whereas μ bumps establish connections between the interposer and chiplet. The modeling of P/G TSVs incorporates resistance, capacitance, and inductance [26], with dimensions specified as 100 μm height, 20 μm diameter, and 200 μm pitch. μ bumps are characterized by inductance and resistance [17], with dimensions of 30 μm in height, 60 μm in diameter, and a pitch of 200 μm . Metal-oxide-semiconductor (MOS) and metal-insulator-metal (MIM) capacitors serve as suitable decap candidates for PDN design. The MOS capacitor can be modeled simply as a capacitor with an equivalent series resistance (ESR). Model parameters for the Uc, P/G TSV, μ bump, and decap based on 55 nm technology are summarized in Table 1. By cascading the UCs, μ bumps, and TSVs, the hierarchical PDNs of 2.5D systems can be modeled.

3.2 Non-Capacitor Zone and Decap Discretization

The small signal noise and SSN can be mitigated by strategically placing the decaps in the PDN. On-chip decaps are typically realized using MOS gate capacitors with small footprints and high capacitance per unit area. For on-interposer PDN, MIM capacitors are often employed due to their cost-effectiveness and ease of fabrication, achieved by incorporating a high-k dielectric medium between the P/G planes. As transistors continue to shrink in size, there is insufficient space within on-chip PDNs to accommodate a large number of MOS capacitors. Consequently, decap distribution tends to concentrate on the interposer. However, there are constraints on decap placement within the interposer. The interposer comprises multiple metal layers, including power, ground, and signal layers. The PDN and MIM capacitors are distributed in the power and ground layers, while chiplet interconnect nets are routed on the RDLs located in the signal layer. Nevertheless, limitations in metal layers may lead to the risk of short circuits if RDL routing intersects with the PDN in the same layer [17]. Moreover, in areas where multiple chiplets converge, signal wires for chiplet intercommunication need to be arranged, further restricting MIM capacitor placement. The area


Figure 3: The target impedance curve.

where MIM capacitors cannot be placed is commonly referred to as the non-capacitor zone.

The smallest cell in which a decap can be placed is referred to as a unit decap cell (UDC), and decaps are positioned within the available layout area of these UDCs. For simplicity and design space reduction, the size of the UDC is set to be 1mm \times 1mm for both the chiplet and interposer. The allowable capacitance for on-interposer MIM capacitors ranges from 200 pF to 2000 pF, with increments of 200 pF. For on-chip MOS capacitors, capacitance values span from 50 pF to 500 pF, with increments of 50 pF.

3.3 Frequency-Domain Impedance Analysis

To ensure a stable voltage supply for the chiplet, the impedance of PDN should remain below the target impedance value within the working frequency range. The target impedance is typically defined as the ratio of the maximum allowable ripple voltage to the half of the maximum transient current I_{max} derived from peak power P_{max} [7], as follows:

$$Z_{target} = \frac{V_{dd} * ripple}{I_{ref}}, \quad I_{max} = \frac{P_{max}}{V_{dd}} \quad (1)$$

here $I_{ref} = \frac{1}{2}I_{max}$ is used to represent the typical workload and avoid over-design. With advancements in transistor manufacturing processes and chip integration, the transistor switching rate is increasing while the amplitude of the maximum transient current is decreasing. Consequently, achieving low impedance at high frequencies becomes unnecessary, as it can lead to over-design and increased costs. Therefore, the target impedance consists of a flat region and a slope region, as depicted in Figure 3. At low frequencies, the target impedance is flat, calculated by (Equation (1)). When the frequency exceeds the keen frequency $f_{knee} = \frac{0.35}{T_r}$, where T_r is the transition time of the signal, the worst transient current decreases at a -20 dB/dec ratio, and likewise, the target impedance curve increases at a rate of 20 dB/dec [27]. In this paper, the *ripple* and f_{knee} are set as 5% and 3.4 GHz respectively.

3.4 Time-Domain VVI Analysis

In the 2.5D system, there are a large number of I/Os between chiplets for signal communication. SSN could propagate through these I/Os, affecting the normal operation of other chiplets. Due to the SSN, the change in transient current during the operating state of the chiplet may exceed the normal operating current, and the waveform and peak value of the current are unpredictable. Therefore, it is difficult to accurately predict whether the voltage noise meets the design requirements solely by frequency-domain analysis

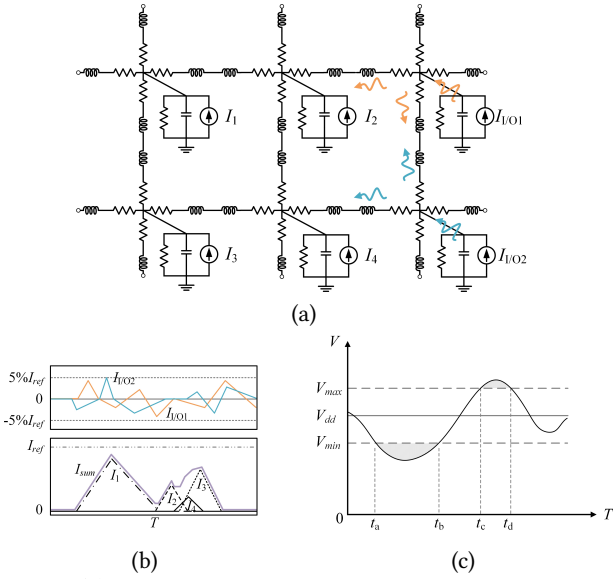


Figure 4: (a) The equivalent circuit of the transient currents. (b) The waveform of the internal currents and I/O currents. (c) Illustration of the voltage violation integral at a node in the V_{dd} power grid.

that inherently a steady-state analysis. To obtain a robust PDN, an evaluation method of PDNs in the time domain is required.

To model the switching current for time-domain evaluation, we employ piecewise linear (PWL) triangular waveform currents with varying peak values and excitation times to simulate the transient current resulting from transistor state switching [22]. The total current of a chiplet can be modeled by superposition of two parts: one is the internal current of the chiplet, and the other is the I/O current fluctuations distributed at the edge of the chiplet, as defined in Eq.(2):

$$\text{Current Model: } \begin{cases} 0 \leq I_{sum}(t) + I_{I/Os}(t) \leq I_{max} \\ I_{sum}(t) = \sum I_{internal}(t) \leq I_{ref}; \\ I_{I/Os}(t) = \left| \sum_i I_{I/Oi}(t) \right| \leq I_{ref}; \\ \int I_{I/Oi}(t) dt = 0 \end{cases} \quad (2)$$

The reference current ($I_{ref} = \frac{1}{2}I_{max}$) is used for transient analysis in consistency with frequency analysis. To maintain overall power consumption within P_{max} limits throughout the simulation, the sum (I_{sum}) of the internal currents are set below I_{ref} and I/O currents can fluctuate within a range of $5\%I_{ref}$ with the peak value of the current summation below I_{ref} . To represent different data transmission scenarios, $I_{I/Oi}$ with different correlations can be specified. Figure 4(a)-(b) illustrate the waveform and the equivalent circuit of the chiplet PDN with transient currents.

To conduct the dynamic power integrity analysis, we introduce the concept of voltage violation integral (VVI), which serves as a measure of the cumulative effect of voltage deviations from specified voltage fluctuations. Figure 4(c) illustrates the voltage violation at a node in the voltage supply V_{dd} power grid. The VVI is represented

by the shaded region and is calculated by

$$VVI = \int_0^T [\max(V_{min} - V(t), 0) + \max(V(t) - V_{max}, 0)] dt \quad (3)$$

where V_{max} and V_{min} represent the maximum and minimum allowable voltages, set to 105% and 95% of the power supply voltage, respectively. As the duration of time during which the voltage exceeds the maximum allowable voltage fluctuation range increases, the likelihood of circuit errors also rises. Considering both the magnitude and duration of voltage deviations, the VVI provides a comprehensive measure of PDN performance, especially in dynamic operating conditions characterized by transient events.

Compared to the methods solely considering the worst-case voltage drop over time [28], the VVI analysis can assess the overall severity of dynamic voltage violations and evaluate the effectiveness of PDN optimization strategies in mitigating SSNs. Thus, minimizing the VVI could ensure the reliability and performance of electronic systems, particularly in high-speed and high-density applications where voltage fluctuations can lead to system failure or performance degradation.

4 Proposed RL-based Decap Optimization Method

In this section, an RL-based method for the hierarchical decap optimization is proposed. The objective of this optimization problem is to minimize the total decap capacitance while ensuring that they meet the target impedance across the desired frequency band and minimize the VVI as much as possible. The proposed algorithm encompasses two steps. Initially, we adjust decap distribution of on-interposer and on-chip PDNs to meet target impedance and limit voltage fluctuation within the ripple range in the frequency domain. Subsequently, in the time domain, we optimize the VVI of on-chip PDN to address the voltage violations induced by SSN propagation.

To handle such a complex problem, we apply deep RL, a machine learning algorithm where an agent learns to make sequential decisions by interacting with an environment to learn a policy that maximizes cumulative rewards by mapping states to actions. This problem can be represented by three key parameters: state, action, and reward. The state captures the configuration of the environment observed by the agent, while the action signifies the decision made by the agent in response to the observed state. For each action, the agent will assign a reward to evaluate the quality of the action and guide the agent's training toward the maximization of reward. The reward reflects the feedback provided by the environment based on the actions taken by the agent. Through iterative interaction with the environment, the agent refines its parameters based on the feedback received.

Figure 5 shows the overall concept of the RL-based approach for optimizing the PDN in chiplet-based 2.5D systems. The algorithm process for decap optimization is detailed in Section 4.1. Furthermore, comprehensive definitions of parameters for impedance optimization and VVI optimization are provided in Section 4.2 and Section 4.3, respectively. The policy network, which plays a pivotal role in determining the actions of action, is represented by a deep neural network (DNN). The structure of the DNN and the specific RL algorithm utilized are expounded upon in Section 4.4.

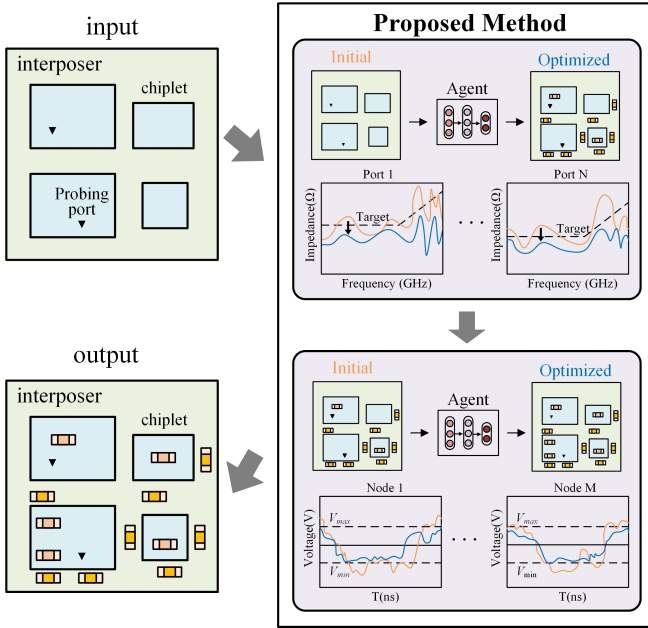


Figure 5: The overall concept of the RL-based method for 2.5D PDN decap optimization.

4.1 Algorithm Process for Decap Optimization

The general algorithm process is described as follows.

- (1) **Early-Stage Floorplanning:** Derive an early-stage floorplanning solution, yielding complete designs for the interposer and chiplets, including placement, routing, and PDNs.
- (2) **Hierarchical PDN Modeling:** Generate hierarchical PDN models in RLGC formats for the 2.5D system, as discussed in Section 3.1.
- (3) **Impedance Analysis:** Perform impedance analysis utilizing the circuit simulator NGSPICE. Optimize the on-chip and on-interposer decaps to meet the target impedance requirements.
- (4) **VVI Optimization:** Simulate the transient currents using the NGSPICE. Subsequently, refine the on-chip decap placement to minimize VVI in the time domain, thereby ensuring optimal performance.

4.2 Matrix Definition Based on Impedance Analysis

For a given hierarchical PDN, the placement of chiplets, the interposer space with non-capacitor zone, the locations and capacitances of MIM capacitors on the interposer PDN, and the locations and capacitances of MOS capacitors on the chiplet PDN, are taken into account for impedance analysis. The information can be encoded into four 2D matrices: Interposer Space Matrix, Chiplet Space Matrix, MIM Distribution Matrix and MOS Distribution Matrix. The dimensions of these matrices are determined by the number of UDCs. The space matrix delineates feasible decap locations on the interposer or chiplet layer and is a binary matrix with '1' indicating feasible positions and '0' denoting non-feasible locations. The capacitor distribution matrix reflects the normalized capacitance values of decaps, with '0' indicating the absence of a unit decap and '1' indicating the presence of a unit decap at the maximum allowable capacitance.

The action is defined as the alteration in capacitance of unit decaps at each timestep. There are ten distinct and incrementally increasing capacitance for both MIM capacitors and MOS capacitors. The action space encompasses all potential combinations of these alterations across all unit decaps of the on-chip and on-interposer PDNs, which can be expressed as:

$$\{-c_{MOS}/c_{MIM}, 0, +c_{MOS}/c_{MIM}\}^{N_{chip}+N_{intp}} \quad (4)$$

Here, c_{MOS} and c_{MIM} represent the capacitance step of the unit MOS capacitor and unit MIM capacitor, respectively. N_{chip} and N_{intp} denote the number of UDCs where the decap can be placed on the chiplet PDNs and interposer PDN, respectively. In this action space, each unit decap can either increase, decrease, or maintain its capacitance unchanged by a certain step size defined by the ratio of c_{MOS} and c_{MIM} .

For the 2.5D system with multiple chiplets, probing ports P are strategically placed across different chiplets to monitor impedance variations. The optimization objective is to ensure that the impedance measured at all probing ports align with the target impedance across the frequency range of interest, while concurrently minimizing the manufacturing cost and the leakage current induced by excessive decaps. We aim for the agent to allocate more capacitance to mitigate impedance when the impedance surpasses the target impedance, and to learn a policy that employs lower capacitance when the impedance aligns with the target impedance. Therefore, the reward function is defined as:

$$R_F = \begin{cases} -\sum_f \max_P(Z(f) - Z_{target}(f)), & \exists Z(f) > Z_{target}(f) \\ \alpha(1 - \frac{\sum C_{mos}}{\sum C_{chipm}}) + \beta(1 - \frac{\sum C_{mim}}{\sum C_{intpm}}), & \forall Z(f) \leq Z_{target}(f) \end{cases} \quad (5)$$

where $Z - Z_{target}$ is the difference between the actual impedance and the target impedance observed at P and f is sampled from 0.1 to 20 GHz, with 100 points per decade in following experiments. $\sum C_{mos}$ and $\sum C_{chipm}$ denote the capacitance of the placed MOS capacitors and the maximum capacitance that can be placed on-chip UDCs, respectively. $\sum C_{mim}$ and $\sum C_{intpm}$ denote the capacitance of the placed MIM capacitors and the maximum capacitance that can be placed on-interposer UDCs. The coefficients α and β are weights, satisfying $\alpha + \beta = 1$. In this context, α and β are both set to 0.5.

4.3 Matrix Definition Based on VVI Analysis

Minimizing VVI is crucial for maintaining stable voltage levels and voltage violation effects, especially in high-performance electronic systems. RL is utilized to adjust PDN decap parameters and minimize VVI, similar to the decap optimization based on impedance analysis. The RL agent learns to optimize the decap configuration of the on-chip PDNs to achieve lower VVI values, building upon impedance optimization. To accomplish this, the VVIs of all on-chip PDN UCs are monitored for optimization. In addition to the PDN information mentioned in Section 4.2, the VVI information of all UCs is also included in the input state matrices as a 2D matrix. This comprehensive information equips the agent to make informed decisions during optimization.

Due to the locality, on-chip decaps are closer to the noise sources, thus more effective in alleviating SSNs. Incorporating this locality

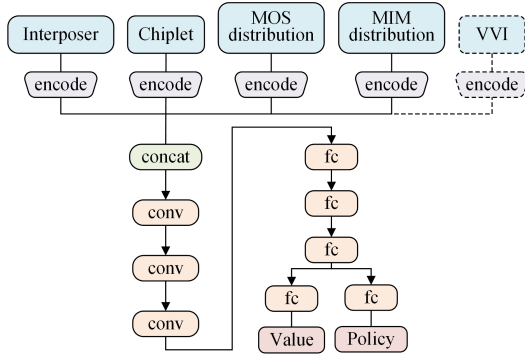


Figure 6: Feature embedding and DNN structure for the proposed RL algorithm, where VVI is only used in the time-domain optimization.

insight, only the on-chip decaps are considered in the following experiments, which could also significantly improve the convergence speed without quality degradation of the final decap distribution. The action space is represented as:

$$\{-c_{MOS}, 0, +c_{MOS}\}^{N_{chip}} \quad (6)$$

Building upon impedance optimization, we incorporate additional capacitors into the on-chip PDNs to alleviate SSN. Our optimization objective is the VVIs of all nodes on the on-chip PDNs, and refining the reward function is necessary. Setting a target value for VVI similar to target impedance is challenging due to the influence of chiplet power, size, and current source distribution. Therefore, we model the reward function to focus on the improvement between initial and optimized VVI. The reward function is expressed as follows:

$$R_T = 1 - \frac{\sum V}{\sum V_{init}} \quad (7)$$

where V_{init} and V represent the VVIs at a node before and after optimization, respectively. This reward function calculates the difference between the ratio of the optimized VVI sum to the initial VVI sum. By employing this reward function, the RL agent aims to maximize the reduction in VVI from its initial state to the optimized state.

4.4 Architecture and RL Algorithm

The architecture of the proposed method, as illustrated in Figure 6, consists of two networks: the policy network and the value network. The policy network determines actions and outputs the probability distribution over available actions based on the current state, while the value network estimates the expected cumulative reward from a given state following the current policy and provides critical feedback to the policy network. Both networks are implemented using a DNN structure. All state matrices are concatenated into a single matrix as the DNN input. The policy network and value network share the same feature extraction layers, which comprise three convolutional layers with 12, 16, and 24 channels, followed by three fully-connected layers. In each convolutional layer, the rectified linear unit (ReLU) function serves as the activation function. The extracted features then pass through a fully-connected layer to generate a probability distribution over actions, which serves as the output of the policy network. Meanwhile, the value network outputs one value representing the goodness of the policy, also through a fully-connected layer.

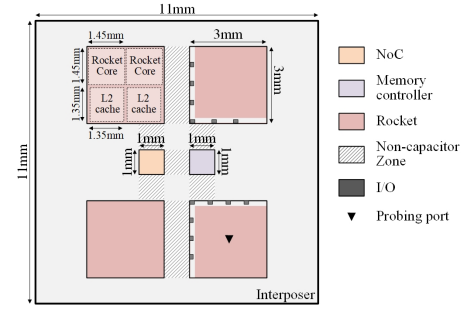


Figure 7: Rocket-64 with the non-capacitor zone. I/Os are evenly distributed at the inner two edges and four probing ports are selected at the center of each Rocket chiplet.

Table 2: Comparisons of different methods in the frequency domain

Method	Proposed Method			DA			GA		
	Reward	MIM (nF)	MOS (nF)	Reward	MIM (nF)	MOS (nF)	Reward	MIM (nF)	MOS (nF)
ROCKET-64	0.545	112.8	7.0	0.439	122.4	10.0	0.329	137.4	12.7
case1	0.578	77.2	11.2	0.523	84.0	13.1	0.494	93.2	13.4
case2	0.646	69.2	7.8	0.578	72.8	10.3	0.575	85.2	9.1
case3	0.619	95.0	7.9	0.576	103.6	9.1	0.537	107.4	10.7
case4	0.537	65.3	5.6	0.429	71.2	7.9	0.397	74.7	8.4
Training Time	~10 hours			>80 hours			>40 hours		
Simulation Steps	1×10^6			3×10^5			5×10^5		

We employ the proximal policy optimization (PPO) [29] algorithm to train the policy and value networks. During training, the agent interacts with the environment, and collects experiences into a replay buffer. Batches of experiences are sampled from this buffer and used to update the policy and value networks. PPO utilizes a clipped surrogate objective function to ensure stable updates and prevent large policy changes. This function constrains the policy updates to be within a certain range, preventing overly aggressive updates that can destabilize training by limiting the extent of policy changes between successive updates. The clipped loss function is formulated as

$$L_t(\theta) = \hat{E}_t[L_t^{CLIP}(\theta) - c_1 L_t^{VF}(\theta) + c_2 S[\pi_\theta](s_t)] \quad (8)$$

$$L^{CLIP}(\theta) = \hat{E}_t[\min(r_t(\theta)\hat{A}_t, \text{clip}(r_t(\theta), 1 - \epsilon, 1 + \epsilon)\hat{A}_t)] \quad (9)$$

$$L_t^{VF}(\theta) = (V(s_t) - V_t^{targ})^2 \quad (10)$$

where $r_t(\theta)$ is the ratio of the new policy and the old policy; ϵ is the clip coefficient; \hat{A}_t is an estimator of the advantage function that represents the difference between the observed rewards and the expected rewards predicted by the value network; L_t^{VF} is a squared-error loss of the value network output; S denotes the entropy of the output probability; c_1 and c_2 are coefficients. In this paper, c_1 and c_2 are both set as 0.5. The Adam optimizer is utilized for training, and the learning rate is established as 10^{-4} .

5 Experiments

To validate our proposed method, we employ five test cases with different PDN configurations, which include ROCKET-64 [30] along with four other synthetic PDNs. The ROCKET-64 configuration comprises six chiplets, including a Network-on-Chip (NoC), a memory controller, and four merged Rockets consisting of two Rocket cores and two L2 Cache units, as illustrated in Figure 7.

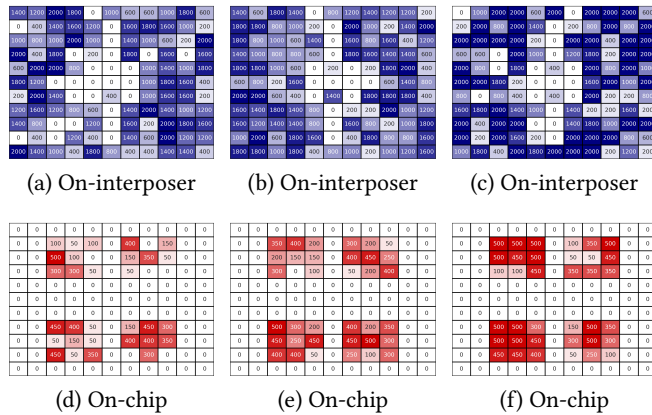


Figure 8: The decap distribution on ROCKET-64 after impedance optimization: (a)(d)the proposed method; (b)(e)DA; (c)(f)GA.

5.1 Frequency-Domain Impedance Optimization

To assess the performance of the proposed RL-based method in the frequency domain, the dual annealing (DA) optimization algorithm, which is an improved simulated annealing algorithm, and genetic algorithm (GA) were selected for comparison. For a fair comparison, the cost functions of the DA and GA were set to the same as the proposed method. Table 2 summarizes the comparison results of different methods on test cases. The reward of the optimal decap design obtained by the proposed method achieved the improvement of 13.01% and 20.29% than the solutions obtained by DA and GA. Moreover, the optimal decap design obtained by the proposed method required lower capacitance values compared to DA and GA. DA and GA took over 80 hours and 40 hours to determine the optimal solutions, while the training time for the proposed method was about 10 hours, representing a significant reduction in training time compared to DA and GA.

The optimal decap distribution on ROCKET-64 is shown in Figure 8. For the on-interposer PDN, the decap distribution obtained by DA occupied almost the entire interposer, while GA tended to place larger capacitance on the interposer PDN. Compared to DA and GA, the proposed method required less layout space to allocate on-interposer decaps, reducing the number of occupied UDCs by 10.18% and 7.41%, respectively, which is more practical for placement and routing. For the on-chip PDNs, the proposed method achieved less capacitance and space occupation than DA and GA. Noted that non-capacitor zone is leaving as blank in all decap distributions. Figure 9 displays the impedance curves at the four probing ports of the initial PDN, located in the center of each Rocket chiplet, and the optimized PDN obtained by different methods. The dashed line represents the target impedance, with a flat region of 35 mΩ and a frequency-dependent increase rate of 20 dB/dec beyond 3.4 GHz. Although all the methods achieved the desired solutions, the optimized PDN obtained by the proposed method avoided over-design with less capacitance, layout space, and design time while satisfying the target impedance across the frequency range of 100 MHz to 20 GHz.

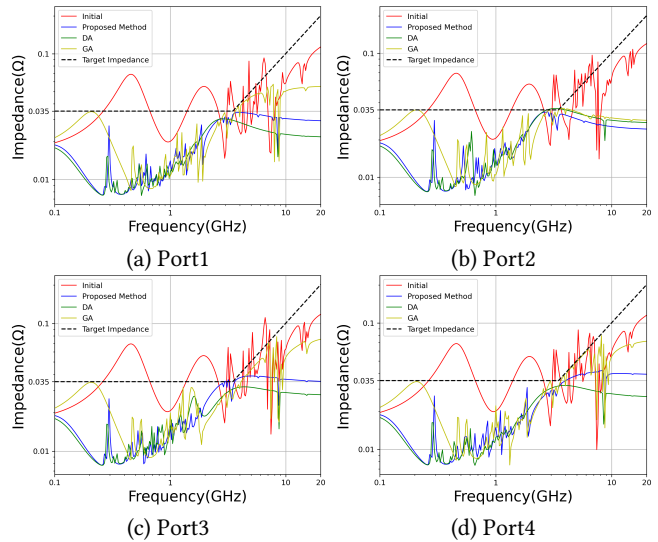


Figure 9: Comparisons of the impedance curves at four ports between the proposed method, DA, and GA.

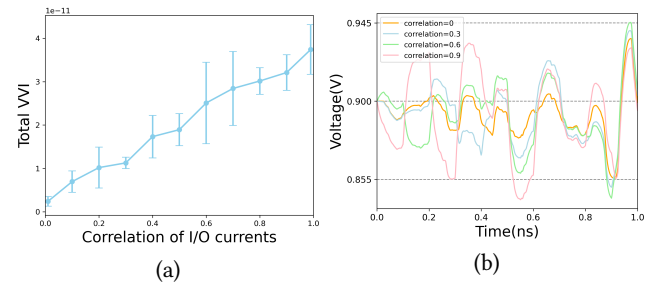


Figure 10: The effect of simultaneous switching: (a) Total VVI variations under different I/O current correlations; (b) Voltage fluctuations of a typical node under different correlations between I/O currents.

5.2 Time-Domain VVI Optimization

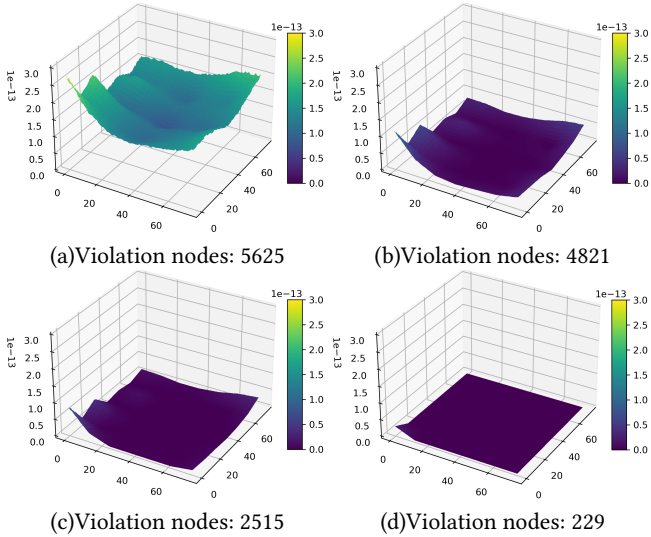
To investigate the voltage violations after frequency-domain optimization, we conducted a time-domain experiment on the ROCKET-64 design. The internal current sources are generated based on the PWL current model and the I_{ref} constrain as described in Equation (2). Then each internal current source is attached to a UC of the PDN to model the normal working condition for Rocket chiplet. Beside internal current sources, thirteen lumped currents sources are distributed evenly at the inner-edges of each Rocket chiplet to model the current fluctuations under high-speed communications, as illustrated in Figure 10(b). Furthermore, the correlation coefficient between I/O current sources is used as a proxy to represent different data transmit patterns of high-speed I/Os. A higher correlation among I/O currents indicates more simultaneous switching of TX/RX circuits, thus more severe the SSN.

Impact of Simultaneous Switching

For correlation coefficients ranging from 0 to 1.0, extensive investigations are conducted with 50 generated current profiles for the post frequency-optimized PDN. The trend and variation of the total VVI of all nodes for 50 cases are summarized in Figure 10(a). Regardless of the correlation level, the total VVI in the 1 ns interval

Table 3: Comparisons before and after time-domain optimization on ROCKET-64

	Total MOS Capacitance	Total VVI	Number of Violation Nodes
Before	7.0 nF	3.297×10^{-11}	22500
After	7.9 nF	2.575×10^{-11}	22500
	9.0 nF	1.757×10^{-11}	22500
	9.9 nF	7.617×10^{-12}	22137
	11.0 nF	4.113×10^{-12}	17924
	12.5 nF	1.210×10^{-12}	9053
	13.6 nF	7.069×10^{-14}	832
	14.9 nF	0	0


Figure 11: VVI Profiles of Rocket chiplet during the time-domain optimization

consistently remains above zero. Thus, we could conclude that even the target impedance has been met at all frequency range, there will still be voltage violations, which cannot be captured solely on frequency-domain analysis.

As the correlation among I/O currents increases, the total VVI also escalates. We selected a typical node of on-chip PDNs to monitor the voltage variation. Under conditions where no simultaneous switching outputs occur within the system, the voltage variation is represented by the orange line in Figure 10(b). Here, the minimum and maximum voltages measure 0.8556 V and 0.9361 V respectively, meeting the specified requirements. However, with an increasing number of signals being switched on and off simultaneously within the system, the voltage fluctuations surpass the 5% voltage ripple limitation of V_{dd} . It is evident that as multiple I/Os switch simultaneously, the voltage fluctuation exceeds permissible levels. This underscores how SSN can indeed impact the power stability of the PDN. Consequently, time-domain optimization becomes imperative to ensure the performance of the 2.5D PDN design.

Results of VVI Optimization

To demonstrate the effectiveness of our time-domain optimization, the VVI results of ROCKET-64 with a I/O correlation of 0.9 was chosen to perform the following optimization. We define the node

where the minimum or maximum voltage over time exceeds the allowable voltage ripple as the violation node. Building upon the frequency-domain optimization, we selected a total of 22500 nodes of ROCKET-64, with each rocket chiplet comprising 5,625 nodes, as additional inputs for the time-domain optimization and further refinement of on-chip decaps by setting the reduction of VVI as the RL optimization objective as in Equation (7). The before and after time-domain optimization results on ROCKET-64 are summarized in Table 3. All nodes that were only optimized in the frequency domain exhibited violations. With the addition of unit MOS capacitors during optimization, the total VVI and violation nodes reduced accordingly. When the total MOS capacitance exceeded 14.9 nF, there were no violation nodes. Figure 11 shows the VVI profile of one Rocket chiplet before and after time-domain optimization. Based on above case study, without losing generality, we have shown the effectiveness of the propose two-phase optimization method to obtain a robust PDN for 2.5D system. In practical design, designers can make a trade-off between the total allowable capacitance and the VVI tolerance to obtain the desired PDN design.

6 Future Work

Promising results have been demonstrated through comprehensive experimental evaluations of the proposed two-phase optimization method. However, there is potential for further improvements that could enhance its effectiveness and establish it as a significant area of research. Firstly, the compact modeling approach of the hierarchical PDN could benefit from cross-verification with more accurate full microwave analyses. This would help determine the optimal frequency range and limitations of the current modeling technique. Additionally, more realistic current models and correlation coefficients should be extracted from SPICE simulations of transmitter/receiver circuits under various workloads. Although the DNN model employed in this study already surpasses traditional DA and GA approaches, exploring more advanced DNN architectures could further improve performance and enhance transferability.

7 Conclusion

In this article, we propose an RL-based method to optimize the decap design of 2.5D hierarchical PDN, incorporating both frequency- and time-domain analyses. Our approach offers greater flexibility in selecting decap types, and consider the constraint of the non-capacitor zone. Through frequency-domain optimization, we successfully meet the target impedance requirements. Subsequent optimization using time-domain techniques notably mitigates SSN. By leveraging a combination of frequency- and time-domain optimization strategies, we significantly enhance power integrity and achieve a robust PDN design. Our experimental results underscore the importance of optimizing PDNs in 2.5D chiplet-based systems, demonstrating the efficacy of our proposed approach.

References

- [1] Furkan Eris, Ajay Joshi, Andrew B. Kahng, Yenai Ma, Saiful Mojumder, and Tiansheng Zhang. Leveraging thermally-aware chiplet organization in 2.5d systems to reclaim dark silicon. In *2018 Design, Automation & Test in Europe Conference & Exhibition (DATE)*, pages 1441–1446, 2018.
- [2] Ajaykumar Kannan, Natalie Enright Jerger, and Gabriel H. Loh. Enabling interposer-based disintegration of multi-core processors. In *2015 48th Annual IEEE/ACM International Symposium on Microarchitecture (MICRO)*, pages 546–558, 2015.
- [3] Madhavan Swaminathan and Ege Engin. *Power integrity modeling and design for semiconductors and systems*. Pearson Education, 2007.

- [4] Jinguok Kim. Statistical analysis for pattern-dependent simultaneous switching outputs (sso) of parallel single-ended buffers. *IEEE Transactions on Circuits and Systems I: Regular Papers*, 64(1):156–169, 2017.
- [5] Shao-Chun Hung, Yi-Chen Lu, Sung Kyu Lim, and Krishnendu Chakrabarty. Power supply noise-aware at-speed delay fault testing of monolithic 3-d ics. *IEEE Transactions on Very Large Scale Integration (VLSI) Systems*, 29(11):1875–1888, 2021.
- [6] Xinchu Xu and Yonggang Wang. Study on voltage influence on fpga-based time-to-digital converters. In *2023 IEEE International Instrumentation and Measurement Technology Conference (I2MTC)*, pages 1–6, 2023.
- [7] L.D. Smith, R.E. Anderson, D.W. Forehand, T.J. Pelc, and T. Roy. Power distribution system design methodology and capacitor selection for modern cmos technology. *IEEE Transactions on Advanced Packaging*, 22(3):284–291, 1999.
- [8] Jinguok Kim, Yuza Takita, Kenji Araki, and Jun Fan. Improved target impedance for power distribution network design with power traces based on rigorous transient analysis in a handheld device. *IEEE Transactions on Components, Packaging and Manufacturing Technology*, 3(9):1554–1563, 2013.
- [9] Stefano Piersanti, Francesco de Paulis, Carlo Olivieri, and Antonio Orlandi. Decoupling capacitors placement for a multichip pdn by a nature-inspired algorithm. *IEEE Transactions on Electromagnetic Compatibility*, 60(6):1678–1685, 2017.
- [10] Francesco de Paulis, Riccardo Cecchetti, Carlo Olivieri, and Markus Buecker. Genetic algorithm pdn optimization based on minimum number of decoupling capacitors applied to arbitrary target impedance. In *2020 IEEE International Symposium on Electromagnetic Compatibility & Signal/Power Integrity (EMCSI)*, pages 428–433. IEEE, 2020.
- [11] Zhifei Xu, Zihao Wang, Yin Sun, Chulsoon Hwang, Hervé Delingette, and Jun Fan. Jitter-aware economic pdn optimization with a genetic algorithm. *IEEE Transactions on Microwave Theory and Techniques*, 69(8):3715–3725, 2021.
- [12] Petr Kadlec, Martin Marek, Martin Štumpf, and Vladimír Šeděnka. Pcb decoupling optimization with variable number of capacitors. *IEEE Transactions on Electromagnetic Compatibility*, 61(6):1841–1848, 2018.
- [13] Surendra Hemaram and Jai Narayan Tripathi. Optimal design of a decoupling network using variants of particle swarm optimization algorithm. In *2021 IEEE International Symposium on Circuits and Systems (ISCAS)*, pages 1–5. IEEE, 2021.
- [14] Shiyu Zhao, Kaushik Roy, and Cheng-Kok Koh. Decoupling capacitance allocation and its application to power-supply noise-aware floorplanning. *IEEE Transactions on Computer-Aided Design of Integrated Circuits and Systems*, 21(1):81–92, 2002.
- [15] Jai Narayan Tripathi, Pratik Damle, and Rakesh Malik. Minimizing core supply noise in a power delivery network by optimization of decoupling capacitors using simulated annealing. In *2017 IEEE 21st Workshop on Signal and Power Integrity (SPI)*, pages 1–3. IEEE, 2017.
- [16] Po-Yang Chen, Chang-Yun Liu, Hung-Ming Chen, and Po-Tsang Huang. On-interposer decoupling capacitors placement for interposer-based 3dic. In *2023 24th International Symposium on Quality Electronic Design (ISQED)*, pages 1–6. IEEE, 2023.
- [17] Changle Zhi, Gang Dong, Yang Wang, Zhangming Zhu, and Yintang Yang. Trade-off-oriented impedance optimization of chiplet-based 2.5-d integrated circuits with a hybrid mdp algorithm for noise elimination. *IEEE Transactions on Circuits and Systems I: Regular Papers*, 69(12):5247–5258, 2022.
- [18] Hyunwook Park, Junyong Park, Subin Kim, Daehwan Lho, Shinyoung Park, Gapyeol Park, Kyungjun Cho, and JoungHo Kim. Reinforcement learning-based optimal on-board decoupling capacitor design method. In *2018 IEEE 27th Conference on Electrical Performance of Electronic Packaging and Systems (EPEPS)*, pages 213–215. IEEE, 2018.
- [19] Hyunwook Park, Junyong Park, Subin Kim, Kyungjun Cho, Daehwan Lho, Seungtaek Jeong, Shinyoung Park, Gapyeol Park, Boogyo Sim, Seongguk Kim, et al. Deep reinforcement learning-based optimal decoupling capacitor design method for silicon interposer-based 2.5-d/3-d ics. *IEEE Transactions on Components, Packaging and Manufacturing Technology*, 10(3):467–478, 2020.
- [20] Hyunwook Park, Minsu Kim, Seongguk Kim, Keunwoo Kim, Haeyeon Kim, Taein Shin, Keeyoung Son, Boogyo Sim, Subin Kim, Seungtaek Jeong, et al. Transformer network-based reinforcement learning method for power distribution network (pdn) optimization of high bandwidth memory (hbm). *IEEE Transactions on Microwave Theory and Techniques*, 70(11):4772–4786, 2022.
- [21] Ling Zhang, Li Jiang, Jack Juang, Zhiping Yang, Er-Ping Li, and Chulsoon Hwang. Decoupling optimization for complex pdn structures using deep reinforcement learning. *IEEE Transactions on Microwave Theory and Techniques*, 2023.
- [22] Haihua Su, S.S. Sapatnekar, and S.R. Nassif. Optimal decoupling capacitor sizing and placement for standard-cell layout designs. *IEEE Transactions on Computer-Aided Design of Integrated Circuits and Systems*, 22(4):428–436, 2003.
- [23] Takashi Enami, Masanori Hashimoto, and Takashi Sato. Decoupling capacitance allocation for timing with statistical noise model and timing analysis. In *2008 IEEE/ACM International Conference on Computer-Aided Design*, pages 420–425, 2008.
- [24] Kyungjun Cho, Youngwoo Kim, Subin Kim, Hyunwook Park, Junyong Park, Seungsoo Lee, Daeyoung Shim, Kangseol Lee, Sangmook Oh, and JoungHo Kim. Fast and accurate power distribution network modeling of a silicon interposer for 2.5-d/3-d ics with multiarray tsvs. *IEEE Transactions on Components, Packaging and Manufacturing Technology*, 9(9):1835–1846, 2019.
- [25] Jiayi He, Chulsoon Hwang, Jingnan Pan, Gyu-Yeong Cho, Bumhee Bae, Hark-Byeong Park, and Jun Fan. Extracting characteristic impedance of a transmission line referenced to a meshed ground plane. In *2016 IEEE International Symposium on Electromagnetic Compatibility (EMC)*, pages 651–656, 2016.
- [26] Kiyeong Kim, Chulsoon Hwang, Kyoungchoul Koo, Jonghyun Cho, Heegon Kim, JoungHo Kim, Junho Lee, Hyung-Dong Lee, Kun-Woo Park, and Jun So Pak. Modeling and analysis of a power distribution network in tsv-based 3-d memory ic including p/g tsvs, on-chip decoupling capacitors, and silicon substrate effects. *IEEE Transactions on Components, Packaging and Manufacturing Technology*, 2(12):2057–2070, 2012.
- [27] Fangyi Rao and Sammy Hindi. Frequency domain analysis of jitter amplification in clock channels. In *2012 IEEE 21st Conference on Electrical Performance of Electronic Packaging and Systems*, pages 51–54, 2012.
- [28] Jinwoo Kim, Venkata Chaitanya Krishna Chekuri, Nael Mizanur Rahman, Majid Ahadi Dolatsara, Hakki Mert Torun, Madhavan Swaminathan, Saibal Mukhopadhyay, and Sung Kyu Lim. Chiplet/interposer co-design for power delivery network optimization in heterogeneous 2.5-d ics. *IEEE Transactions on Components, Packaging and Manufacturing Technology*, 11(12):2148–2157, 2021.
- [29] John Schulman, Filip Wolski, Prafulla Dhariwal, Alec Radford, and Oleg Klimov. Proximal policy optimization algorithms. *arXiv preprint arXiv:1707.06347*, 2017.
- [30] Jinwoo Kim, Gauthaman Murali, Heechun Park, Eric Qin, Hyoukjun Kwon, Venkata Chaitanya Krishna Chekuri, Nihar Dasari, Arvind Singh, Minah Lee, Hakki Mert Torun, Madhavan Swaminathan, Madhavan Swaminathan, Saibal Mukhopadhyay, Tushar Krishna, and Sung Kyu Lim. Architecture, chip, and package co-design flow for 2.5d ic design enabling heterogeneous ip reuse. In *2019 56th ACM/IEEE Design Automation Conference (DAC)*, pages 1–6, 2019.